INTERNATIONAL JOURNAL OF
NUMERICAL ANALYSIS AND MODELING
Volume 22, Number 6, Pages 755–776

doi: 10.4208/ijnam2025-1033

MEAN SQUARE STABILITY OF NUMERICAL METHOD FOR STOCHASTIC VOLTERRA INTEGRAL EQUATIONS WITH DOUBLE WEAKLY SINGULAR KERNELS

OMID FARKHONDEH ROUZ, SEDAGHAT SHAHMORAD, AND FEVZI ERDOGAN

Abstract. The main goal of this paper is to develop an improved stochastic θ-scheme as a numerical method for stochastic Volterra integral equations (SVIEs) with double weakly singular kernels and demonstrate that the stability of the proposed scheme is affected by the kernel parameters. To overcome the low computational efficiency of the stochastic θ-scheme, we employed the sum-of-exponentials (SOE) approximation. Then, the mean square stability of the proposed scheme with respect to a convolution test equation is studied. Additionally, based on the stability conditions and the explicit structure of the stability matrices, analytical and numerical stability regions are plotted and compared with the split-step θ-method and the θ-Milstein method. The results confirm that our approach aligns significantly with the expected physical interpretations.

Key words. Stochastic Volterra integral equations, weakly singular kernels, stochastic θ-scheme, SOE approximation, mean square stability.

1. Introduction

It is well known that a stochastic Volterra integral equation (SVIE) may be generalized from a stochastic differential equation (SDE) [28]-[33] or a standard Volterra integral equation [4, 16, 17, 42]. Equations of these kinds are often used in many scientific fields. For instance, they are often employed in the modelling of biological systems [18], financial markets [9, 13], control science [3], engineering [8] and health care [15]. Since a closed-form solution for SVIEs is generally not available, stochastic numerical schemes offer reliable techniques for studying the behavior of solutions [39, 45, 46, 50, 51]. Therefore, stochastic numerical analysis is a special area of interest in the study of SVIEs [1]. Moreover, the stochastic integral term in the equation commonly lacks a martingale property, leading to a non-Markovian process for the equation's solution. This non-Markovian behavior arises due to the dependence of SVIE kernels on the variable t. As a result, SVIEs are more demanding to analyze and solve in some ways than SDEs, and the accompanying numerical analysis is likewise more challenging. SVIEs with smooth kernels are now supported by the majority of numerical approximations. For example, Xiao et al. [6] presented a collocation method with split-step for SVIEs. Liang et al. [25] presented the Euler–Maruyama method for linear SVIEs of strong convergence with order $\frac{1}{2}$. In [24], the authors presented the modified stochastic θ-methods for the numerical integration of SVIEs.

However, fractional Brownian motion research and the discussion of specific problems in the area of stochastic partial differential equations (SPDEs) are two areas where SVIEs with singular kernels can be identified [44]. The singularity of the kernel at both limits of integral poses the biggest obstacle to implementing stochastic numerical approximations. Zhang [48] peruse the convergence of Euler Maruyama (EM) scheme with the property of large deviations for SVIEs with singular kernel. Xiao [49] find out the convergence order for SVIEs under the EM method with

Received by the editors on May 2, 2024 and, accepted on February 25, 2025.
2000 *Mathematics Subject Classification.* 45D05, 45G05, 60H20, 65C30.

the feature of Abel-type kernels. Wang [47] proved an existence and uniqueness theorem under non-Lipschitz, linear growth condition, and a few integrable conditions. In particular, Li et al. [19] offered two numerical schemes for solving weakly singular SVIEs and extracted strong convergence rates for both of them.

Due to the singularity of the integrand, both integral limits present additional challenges. Unfortunately, the essential Itô formula, a powerful tool in studying SDEs, is not accessible in this research. Thus, we must embark on a search for alternative methods. For instance, Li et al. [41] used the Gronwall inequality to analyze the precise asymptotic separation rate of two alternative double singular SVIE solutions, each with two different initial data. In order to solve the SVIEs with double singular kernels, Li et al. [5] proposed the Galerkin approximation and proved strong convergence rates. Dai and Xiao [38] take into account nonlinear SVIEs with double weakly singular kernels. The d-dimensional SVIE with double weakly singular kernels is taken into consideration in this study as:

(1)
$$y(t) = y_0 + \int_0^t (t-s)^{-\gamma_1} s^{-\sigma_1} F(y(s))ds + \int_0^t (t-s)^{-\gamma_2} s^{-\sigma_2} G(y(s))dW(s), \quad t \in [0,T],$$

where

- The functions $F : \mathbb{R}^d \to \mathbb{R}^d$ and $G : \mathbb{R}^d \to \mathbb{R}^{d\times r}$ are nonlinear Borel measurable, and the initial data $y_0 \in \mathbb{R}^d$ satisfies $\mathbb{E}\big(|y_0|^2\big) < +\infty$.
- The r-dimensional Wiener process $\{W(t)\}_{t\in[0,T]}$ is defined on a complete filtered probability space.
- For $i = 1, 2$, the parameters γ_i and σ_i are non-negative, satisfying $0 < \gamma_1 + \sigma_1 < 1$, and $0 < \gamma_2 + \sigma_2 < \frac{1}{2}$.

For SVIEs (1) no results have been found regarding the stability of the analytical solution. Therefore, we conclude that by utilizing the SOE approximation, we analyze the mean square stability of the suggested scheme. However, numerical approximations for SVIEs with double singular kernels require the storage and utilization of the entire solution history throughout the calculation process. This significantly increases the computational and memory costs. For instance, the EM method has an average storage requirement of $\mathcal{O}(N)$ and an overall calculation cost of $\mathcal{O}(N^2)$. Therefore, it is crucial to find ways to reduce the computational costs. The aim behind the SOE approximation, which is used to approximate the kernel functions, is to reduce the computational complexity and memory cost of the numerical schemes [7, 10]. Hairer et al. [35] used fast Fourier transform techniques and the convolution structure to quickly solve nonlinear Volterra convolution equations. In order to overcome the poor computing efficiency, the SOE approximation was used by Dai and Xiao [38] to offer a fast EM method for double singular kernels in Levy-driven SVIEs. Wang et al. [20] proved the stability and convergence analysis of fast θ-Maruyama scheme for SVIEs of convolution type. Additionally, stability analysis of numerical methods for SVIEs, including the split-step θ-method [4], the θ-method [23] and the improved stochastic θ-method [24] has been thoroughly studied. Furthermore, the convergence analysis is the primary focus of the research on numerical approaches for SVIEs. We are aware of very little information regarding the analytical and numerical stability characteristics of SVIEs with singular kernels. To duplicate the mean square stability of the analytical solution, Doan et al. [40] developed an exponential EM method. Tuan [26] investigated the asymptotic mean square stability of solutions to SVIEs driven by a multiplicative white noise. As a result, by utilizing the SOE approximation, the scheme outlined in

this paper is able to significantly decrease computational expenses and storage demands to $\mathcal{O}(N\log N)$ and $\mathcal{O}(\log N)$ when $T \gg 1$, respectively. Furthermore, when $T \approx 1$, the computational cost and storage requirements are further diminished to $\mathcal{O}(N\log^2 N)$ and $\mathcal{O}(\log^2 N)$, respectively.

The structure of the remaining parts is as follows: Section 2 presents the necessary notations. The main objective of Section 3 is to establish the stochastic θ-scheme, employing the SOE approximation, with the primary goal of reducing computational costs and storage requirements efficiently. The mean square stability characteristics of the proposed scheme are derived in Section 4. Section 5 offers two numerical experiments demonstrating full agreement with the theoretical findings presented in Section 4. The summary of this work is provided in Section 6.

2. Preliminaries

In this paper, we refer to $|\cdot|$ as the Euclidean norm $|y| = \big(\sum_{i=0}^{d} y_i^2\big)^{\frac{1}{2}}$ for $y \in \mathbb{R}^d$ and $\|\cdot\|$ denotes the trace norm of a matrix $\|A\| = \sqrt{trace(A^TA)}$ for $A \in \mathbb{R}^{d\times r}$. Consider $(\Omega, \mathcal{F}, \mathbb{P})$ as a complete probability space with a filtration $\{\mathcal{F}_t\}_{t\geq 0}$ that satisfies common assumptions.

Assumption 2.1. *The functions F and G satisfy the following conditions:*

- ***(Global Lipschitz condition)*** *there exists a constant $L > 0$ such that:*

$$|F(y_1) - F(y_2)|^2 \vee \|G(y_1) - G(y_2)\|^2 \leq L|y_1 - y_2|^2, \quad \forall y_1, y_2 \in \mathbb{R}^d. \tag{2}$$

- ***(Linear growth condition)*** *there exists a constant $K > 0$ such that:*

$$|F(y)|^2 \vee \|G(y)\|^2 \leq K(1 + |y|^2), \quad \forall y \in \mathbb{R}^d. \tag{3}$$

Assumption 2.2. *Define the recurrence relation:*

$$C_{m+1} = C_m \frac{\Gamma\big(m(1-\gamma-\sigma)+1-\sigma\big)}{\Gamma\big(m(1-\gamma-\sigma)+2-\gamma-\sigma\big)}, \quad m = 0, 1, 2, \cdots, \tag{4}$$

with $C_0 = 1$, where $\Gamma(u) = \int_0^\infty z^{u-1}\exp(-z)dz$, $u > 0$ denotes the Gamma function. Define:

$$E_{1-\gamma,1-\sigma}(s) = \sum_{m=0}^{\infty} C_m s^{m(1-\gamma-\sigma)}, \tag{5}$$

which is closely related to the Mittag-Leffler function [36].

Remark 2.1. *We shall use the following asymptotic property of the function $E_{1-\gamma,1-\sigma}$ for similar property of the Mittag-Leffler function* [37]*:*

$$E_{1-\gamma,1-\sigma}(s) = \mathcal{O}\Big(s^{\frac{1}{2}\left(\frac{1-\gamma-\sigma}{1-\gamma}-1+\sigma\right)}\exp\Big(\frac{1-\gamma}{1-\gamma-\sigma}s^{\frac{1-\gamma-\sigma}{1-\gamma}}\Big)\Big), \quad \text{as } s \to \infty. \tag{6}$$

Definition 2.1. [14] *Let $\lambda \neq 0$, $-1 < \gamma < 1$ and σ be a real number. There exist positive constants $M(\gamma,\sigma)$ and $\hat{M}(\gamma)$ depending on γ and σ such that for any $t \geq 0$, it holds that if $\sigma \neq \gamma$, then:*

$$|E_{\gamma+1,\sigma+1}(\lambda t^{\gamma+1})| \leq \frac{M(\gamma,\sigma)}{|\lambda|\max\{1, t^{\gamma+1}\}}. \tag{7}$$

Moreover, if $\sigma = \gamma$, then we can obtain:

$$|E_{\gamma+1,\gamma+1}(\lambda t^{\gamma+1})| \leq \frac{\hat{M}(\gamma)}{\lambda^2 \max\{1, t^{2(\gamma+1)}\}}. \tag{8}$$

The SOE approximation is an important technique for approximating kernel functions using a linear combination of exponential functions. Now, we can derive the following lemma based on the explanation of the SOE approximation [7].

Lemma 2.1. *For every $\gamma \in (0,1)$, there exist positive quadrature nodes τ_l and weights ω_l, $l = 1, 2, \ldots, M_{\exp}$, along with an absolute tolerance error $\epsilon \ll 1$ and a cut-off time point δ, such that:*

$$|t^{-\gamma} - \sum_{l=1}^{M_{\exp}} \omega_l e^{-\tau_l t}| \leq \epsilon, \quad \forall t \in [\delta, T], \tag{9}$$

where the number of exponential terms $M_{\exp}$ needed is of the order:

$$M_{\exp} = \mathcal{O}\Big(\log \frac{1}{\epsilon} \big(\log\log \frac{1}{\epsilon} + \log \frac{T}{\delta} \big) + \log \frac{1}{\delta} \big(\log\log \frac{1}{\epsilon} + \log \frac{1}{\delta} \big) \Big). \tag{10}$$

In other words, if we use the cut-off time $\delta = h$ for a fixed precision ϵ, then we obtain:

$$M_{\exp} = \begin{cases} \mathcal{O}(\log N), & \text{if} \quad T \gg 1, \\ \mathcal{O}(\log^2 N), & \text{if} \quad T \approx 1, \end{cases}$$

where $h = \frac{T}{N}$ (see [[21], pp. 652]).

3. Improved stochastic θ-scheme

In this section, we offer a modified version of the Euler-Maruyama approximation that eliminates the requirement to model extra stochastic integrals in the actual numerical implementation. Let $I_h =: \{t_n := nh : \ n = 0, 1, \ldots, N\}$ be a partition of $I = [0, T]$, then we can approximate Eq. (1) as follows:

$$\begin{aligned} y(t_n) &= y_0 + \int_0^{t_n} (t_n - s)^{-\gamma_1} s^{-\sigma_1} F(y(s)) ds + \int_0^{t_n} (t_n - s)^{-\gamma_2} s^{-\sigma_2} G(y(s)) dW(s) \\ &= y_0 + \theta \int_0^{t_n} (t_n - s)^{-\gamma_1} s^{-\sigma_1} F(y(s)) ds \\ &+ (1-\theta) \int_0^{t_n} (t_n - s)^{-\gamma_1} s^{-\sigma_1} F(y(s)) ds + \int_0^{t_n} (t_n - s)^{-\gamma_2} s^{-\sigma_2} G(y(s)) dW(s) \\ &\approx y_0 + \theta \sum_{k=0}^{n-1} (t_n - t_k)^{-\gamma_1} t_{k+1}^{-\sigma_1} F(y(t_{k+1})) h \\ &+ (1-\theta) \sum_{k=0}^{n-1} (t_n - t_k)^{-\gamma_1} t_{k+1}^{-\sigma_1} F(y(t_k)) h + \sum_{k=0}^{n-1} (t_n - t_k)^{-\gamma_2} t_{k+1}^{-\sigma_2} G(y(t_k)) \Delta W_k, \end{aligned} \tag{11}$$

where $\theta \in [0, 1]$, $n = 1, 2, \ldots, N$ and $\Delta W_k := W_{t_{k+1}} - W_{t_k}$ is the increment of Wiener process. The stochastic θ-scheme for double singular SVIEs (1) can be adjusted to

avoid discarding singular points of kernel functions as:

$$Y_n = y_0 + \theta \sum_{k=0}^{n-1} (t_n - t_k)^{-\gamma_1} t_{k+1}^{-\sigma_1} F(Y_{k+1}) h + (1-\theta) \sum_{k=0}^{n-1} (t_n - t_k)^{-\gamma_1} t_{k+1}^{-\sigma_1} F(Y_k) h$$

$$+ \sum_{k=0}^{n-1} (t_n - t_k)^{-\gamma_2} t_{k+1}^{-\sigma_2} G(Y_k) \Delta W_k. \tag{12}$$

Note that $Y_n := y(t_n)$. Now, by utilizing the SOE approximation (9) to achieve the primary stability analysis, the proposed scheme (12) can be restructured as follows:

$$\begin{aligned} Y_n = y_0 &+ \theta \sum_{k=0}^{n-1} \sum_{l=1}^{M_{\exp,1}} w_{l,1} e^{-\tau_{l,1}(t_n - t_k)} t_{k+1}^{-\sigma_1} F(Y_{k+1}) h \\ &+ (1-\theta) \sum_{k=0}^{n-1} \sum_{l=1}^{M_{\exp,1}} w_{l,1} e^{-\tau_{l,1}(t_n - t_k)} t_{k+1}^{-\sigma_1} F(Y_k) h \\ &+ \sum_{k=0}^{n-1} \sum_{l=1}^{M_{\exp,2}} w_{l,2} e^{-\tau_{l,2}(t_n - t_k)} t_{k+1}^{-\sigma_2} G(Y_k) \Delta W_k, \end{aligned} \tag{13}$$

where $(t_n - t_k)^{-\gamma_1}$ and $(t_n - t_k)^{-\gamma_2}$ are replaced by $\sum_{l=1}^{M_{\exp,j}} w_{l,j} e^{-\tau_{l,j}(t_n - t_k)}$, $j = 1, 2$, respectively. In addition, Eq. (13) can be rewritten as:

$$Y_n = y_0 + \theta \sum_{l=1}^{M_{\exp,1}} w_{l,1} P_{1,l}(t_n) + (1-\theta) \sum_{l=1}^{M_{\exp,1}} w_{l,1} P_{2,l}(t_n) + \sum_{l=1}^{M_{\exp,2}} w_{l,2} P_{3,l}(t_n), \tag{14}$$

where

$$\begin{aligned} P_{1,l}(t_n) &= h \sum_{k=0}^{n-1} e^{-\tau_{l,1}(t_n - t_k)} t_{k+1}^{-\sigma_1} F(Y_{k+1}), \\ P_{2,l}(t_n) &= h \sum_{k=0}^{n-1} e^{-\tau_{l,1}(t_n - t_k)} t_{k+1}^{-\sigma_1} F(Y_k), \\ P_{3,l}(t_n) &= \sum_{k=0}^{n-1} e^{-\tau_{l,2}(t_n - t_k)} t_{k+1}^{-\sigma_2} G(Y_k) \Delta W_k. \end{aligned} \tag{15}$$

This suggests that the cost of calculation drops from $\mathcal{O}(N^2)$ to $\mathcal{O}\big(NM_{\exp}\big) = \begin{cases} \mathcal{O}(N \log N), & \text{if} \quad T \gg 1, \\ \mathcal{O}(N \log^2 N), & \text{if} \quad T \approx 1. \end{cases}$

Remark 3.1. *The combination of Lemma 2.1 and the stochastic θ-scheme* (12) *demonstrates that the computational cost and storage requirements for a single sample are reduced from $\mathcal{O}(N^2)$ and $\mathcal{O}(N)$ to $\mathcal{O}(N \log N)$ and $\mathcal{O}(\log N)$, respectively when $T \gg 1$. For $T \approx 1$, the reductions are to $\mathcal{O}(N \log^2 N)$ and $\mathcal{O}(\log^2 N)$, respectively. For more information, we refer the interested reader to* [7].

4. Mean square stability analysis

In this section, we will primarily concentrate on time discretization of linear SVIEs with double singular kernels. Subsequently, we will analyze the mean square stability of the proposed scheme to ensure its effectiveness. Let us consider the test equation as follows:

(16)
$$y(t) = y_0 + \lambda \int_0^t (t-s)^{-\gamma_1} s^{-\sigma_1} y(s) ds + \mu \int_0^t (t-s)^{-\gamma_2} s^{-\sigma_2} y(s) dW(s), \qquad t \geq 0,$$

where $0 < \gamma_1 + \sigma_1 < 1$, $0 < \gamma_2 + \sigma_2 < \frac{1}{2}$ and $\lambda, \mu \in \mathbb{R}$. Based on the variation of constant formula the test Eq. (16) can be rewritten as follows [22]:

$$\begin{aligned} y(t) &= E_{1-\gamma_1,1-\sigma_1}\big(\lambda\Gamma(2-\gamma_1-\sigma_1)t^{1-\gamma_1-\sigma_1}\big)y_0 \\ &\quad + \mu\Gamma(2-\gamma_2-\sigma_2)\int_0^t (t-s)^{-\gamma_2}s^{-\sigma_2}E_{1-\gamma_2,1-\sigma_2} \\ &\quad \cdot \big(\lambda\Gamma(2-\gamma_1-\sigma_1)(t-s)^{-\gamma_1}s^{-\sigma_1}\big)y(s)dW(s), \end{aligned} \tag{17}$$

where Γ is the Gamma function and the function $E_{1-\gamma,1-\sigma}$ is defined by relation (5).

Lemma 4.1. [43] *Suppose that $\lambda \neq 0$ and $\gamma + \sigma \in (0,1)$. There exists positive constant $M(\gamma,\sigma)$ depending on γ and σ such that for any $t \geq 0$, it holds that if $\gamma \neq \sigma$, then:*

$$|E_{1-\gamma,1-\sigma}\big(\lambda t^{1-\gamma-\sigma}\big)| \leq \frac{M(\gamma,\sigma)}{|\lambda|\max\{1, t^{1-\gamma-\sigma}\}}. \tag{18}$$

Also, let $1-2\gamma+2\sigma > 0$ and $\alpha \in (0, -\gamma+\sigma+\frac{1}{2})$ be arbitrary, then we have:

$$\begin{aligned} &\limsup_{t\to\infty} \Big(\mu\Gamma(2-\gamma-\sigma)\Big)^2 \int_0^t (t-s)^{-2\gamma}s^{-2\sigma} \\ &\cdot \Big(E_{1-\gamma,1-\sigma}\big(\lambda\Gamma(2-\gamma-\sigma)(t-s)^{-\gamma}s^{-\sigma}\big)\Big)^2 \frac{\max\{1,t^{2\alpha}\}}{\max\{1,s^{2\alpha}\}}ds < 1. \end{aligned} \tag{19}$$

The stability result of Eq. (17) is given in the following theorem.

Theorem 4.1. *Suppose that the conditions*

$$\lambda < 0 \quad \textit{and}$$

$$\Big(\mu\Gamma(2-\gamma_2-\sigma_2)\Big)^2 \int_0^\infty s^{-2(\gamma_2+\sigma_2)}\Big(E_{1-\gamma_2,1-\sigma_2}\big(\lambda\Gamma(2-\gamma_1-\sigma_1)s^{-(\gamma_1+\sigma_1)}\big)\Big)^2 ds < 1, \tag{20}$$

hold, then for $1-2(\gamma_1+\sigma_1)+2(\gamma_2+\sigma_2) > 0$ and $\alpha \in \big(0, -(\gamma_1+\sigma_1)+(\gamma_2+\sigma_2)+\frac{1}{2}\big)$ when $\gamma_1+\sigma_1 \neq \gamma_2+\sigma_2$, the solution $y(t)$ of Eq. (16) satisfies the property:

$$\lim_{t\to\infty} t^\alpha \mathbb{E}|y(t)|^2 = 0, \tag{21}$$

which implies the mean square asymptotical stability property of Eq. (16), i.e., $\mathbb{E}|y(t)|^2 \to 0$ when $t \to \infty$.

Proof. Let us consider the case of $\gamma_1+\sigma_1 \neq \gamma_2+\sigma_2$. By choosing $\hat{\alpha} \in \big(\alpha, -(\gamma_1+\sigma_1)+(\gamma_2+\sigma_2)+\frac{1}{2}\big)$, it is sufficient to show that:

$$\limsup_{t\to\infty} t^{2\hat{\alpha}} \frac{\mathbb{E}|y(t)|^2}{\mathbb{E}|y_0|^2} < \infty. \tag{22}$$

We are now proving the inequality (22) by contradiction. Then, there exists an increasing sequence $\{t_n\}$ tending to ∞ such that:

$$\psi_n := \max\{1, t_n^{2\hat{\alpha}}\}\frac{\mathbb{E}|y(t)|^2}{\mathbb{E}|y_0|^2}, \tag{23}$$

satisfies

$$\psi_n = \max\Big\{\max\{1, t_n^{2\hat{\alpha}}\}\frac{\mathbb{E}|y(t)|^2}{\mathbb{E}|y_0|^2} : \quad t \in [0, t_n]\Big\}, \tag{24}$$

and $\lim_{n\to\infty}\psi_n = \infty$. Replacing $t = t_n$ in Eq. (17) and by virtue of Lemma 4.1, we arrive at:

$$\begin{aligned}\frac{\mathbb{E}|y(t_n)|^2}{\mathbb{E}|y_0|^2} &\le \frac{M(\gamma_2,\sigma_2)}{|\lambda|\max\{1, t_n^{2-\gamma_2+\sigma_2}\}} + \Big(\mu\Gamma(2-\gamma_2-\sigma_2)\Big)^2 \\ &\cdot \int_0^{t_n}(t_n-s)^{-2(\gamma_2+\sigma_2)}\Big(E_{1-\gamma_2,1-\sigma_2}\big(\lambda\Gamma(2-\gamma_1-\sigma_1)(t_n-s)^{-(\gamma_1+\sigma_1)}\big)\Big)^2\frac{\mathbb{E}|y(s)|^2}{\mathbb{E}|y_0|^2}ds,\end{aligned} \tag{25}$$

which implies that:

$$\begin{aligned}\psi_n &\le \frac{M(\gamma_2,\sigma_2)\max\{1, t_n^{2\hat{\alpha}}\}}{|\lambda|\max\{1, t_n^{2-\gamma_2+\sigma_2}\}} + \psi_n\Big(\mu\Gamma(2-\gamma_2-\sigma_2)\Big)^2\int_0^{t_n}(t_n-s)^{-2(\gamma_2+\sigma_2)} \\ &\cdot \Big(E_{1-\gamma_2,1-\sigma_2}\big(\lambda\Gamma(2-\gamma_1-\sigma_1)(t_n-s)^{-(\gamma_1+\sigma_1)}\big)\Big)^2\frac{\max\{1, t_n^{2\hat{\alpha}}\}}{\max\{1, s^{2\hat{\alpha}}\}}ds.\end{aligned} \tag{26}$$

Therefore, we can obtain:

$$\begin{aligned}&\psi_n\Big(1 - \big(\mu\Gamma(2-\gamma_2-\sigma_2)\big)^2\int_0^{t_n}(t_n-s)^{-2(\gamma_2+\sigma_2)} \\ &\cdot \big(E_{1-\gamma_2,1-\sigma_2}\big(\lambda\Gamma(2-\gamma_1-\sigma_1)(t_n-s)^{-(\gamma_1+\sigma_1)}\big)\big)^2\frac{\max\{1, t_n^{2\hat{\alpha}}\}}{\max\{1, s^{2\hat{\alpha}}\}}ds\Big) \\ &\le \frac{M(\gamma_2,\sigma_2)\max\{1, t_n^{2\hat{\alpha}}\}}{|\lambda|\max\{1, t_n^{2-\gamma_2+\sigma_2}\}}.\end{aligned} \tag{27}$$

Since $2\hat{\alpha} < 1 - 2(\gamma_2+\sigma_2) + 2(\gamma_1+\sigma_1) < 2(\gamma_1+\sigma_1+1)$, it follows that:

$$\lim_{t\to\infty}\sup\frac{M(\gamma_2,\sigma_2)\max\{1, t_n^{2\hat{\alpha}}\}}{|\lambda|\max\{1, t_n^{2-\gamma_2+\sigma_2}\}} = 0, \tag{28}$$

which contradicts to the definition of $\lim_{n\to\infty}\psi_n = \infty$ and Lemma 4.1. The proof is complete. □

Now, based on Eq. (12), the stochastic θ-scheme for the test Eq. (16) with $0 < \gamma_1 + \sigma_1 < 1$ and $0 < \gamma_2 + \sigma_2 < \frac{1}{2}$ can be expressed as:

$$\begin{aligned}Y_n &= y_0 + \theta\lambda h\sum_{k=0}^{n-1}(t_n-t_k)^{-\gamma_1}t_{k+1}^{-\sigma_1}Y_{k+1} + (1-\theta)\lambda h\sum_{k=0}^{n-1}(t_n-t_k)^{-\gamma_1}t_{k+1}^{-\sigma_1}Y_k \\ &+ \mu\sqrt{h}\sum_{k=0}^{n-1}(t_n-t_k)^{-\gamma_2}t_{k+1}^{-\sigma_2}Y_k\eta_k,\end{aligned} \tag{29}$$

where we have replaced the Wiener increments $W(t_k+h) - W(t_k)$ by the scaled random variables $\sqrt{h}\eta_k$ and η_k represents a standard Gaussian random variable, indicating that every η_k follows a $N(0,1)$-distribution. However, due to the singularity of $(t_n-t_k)^{-\gamma}t_{k+1}^{-\sigma}$ the same approach cannot be directly applied to the proposed scheme for the test Eq. (16). In order to address this issue, the SOE

approximation (9) is incorporated into Eq. (29), enabling the desired outcome to be achieved.

$$\begin{aligned} Y_n = y_0 &+ \theta\lambda h \sum_{k=0}^{n-1} \sum_{l=1}^{M_{\exp,1}} w_{l,1} e^{-\tau_{l,1}(t_n - t_k)} t_{k+1}^{-\sigma_1} Y_{k+1} \\ &+ (1-\theta)\lambda h \sum_{k=0}^{n-1} \sum_{l=1}^{M_{\exp,1}} w_{l,1} e^{-\tau_{l,1}(t_n - t_k)} t_{k+1}^{-\sigma_1} Y_k \\ &+ \mu\sqrt{h} \sum_{k=0}^{n-1} \sum_{l=1}^{M_{\exp,2}} w_{l,2} e^{-\tau_{l,2}(t_n - t_k)} t_{k+1}^{-\sigma_2} Y_k \eta_k. \end{aligned} \tag{30}$$

Let:

$$\tilde{P}_{1,l}(t_n) := \sum_{k=0}^{n-1} e^{-\tau_{l,1}(t_n - t_k)} t_{k+1}^{-\sigma_1} Y_{k+1}, \tag{31}$$

$$\tilde{P}_{2,l}(t_n) := \sum_{k=0}^{n-1} e^{-\tau_{l,1}(t_n - t_k)} t_{k+1}^{-\sigma_1} Y_k, \tag{32}$$

$$\tilde{P}_{3,l}(t_n) := \sum_{k=0}^{n-1} e^{-\tau_{l,2}(t_n - t_k)} t_{k+1}^{-\sigma_2} Y_k. \tag{33}$$

Now, by substituting (31)-(33) into (30), we derive:

$$\begin{aligned} Y_n = y_0 &+ \theta\lambda h \sum_{l=1}^{M_{\exp,1}} w_{l,1} \tilde{P}_{1,l}(t_n) \\ &+ (1-\theta)\lambda h \sum_{l=1}^{M_{\exp,1}} w_{l,1} \tilde{P}_{2,l}(t_n) + \mu\sqrt{h} \sum_{l=1}^{M_{\exp,2}} w_{l,2} \tilde{P}_{3,l}(t_n)\eta_n, \end{aligned} \tag{34}$$

which is the improved stochastic θ-scheme for Eq. (16) with double singular kernels. Note that $\tilde{P}_{1,l}$, $\tilde{P}_{2,l}$, and $\tilde{P}_{3,l}$ denote the characteristic properties of exponential functions, defined by:

$$\tilde{P}_{1,l}(t_n) = e^{-\tau_{l,1}h} \tilde{P}_{1,l}(t_{n-1}) + e^{-\tau_{l,1}h} t_n^{-\sigma_1} Y_n, \tag{35}$$

$$\tilde{P}_{2,l}(t_n) = e^{-\tau_{l,1}h} \tilde{P}_{2,l}(t_{n-1}) + e^{-\tau_{l,1}h} t_n^{-\sigma_1} Y_{n-1}, \tag{36}$$

$$\tilde{P}_{3,l}(t_n) = e^{-\tau_{l,2}h} \tilde{P}_{3,l}(t_{n-1}) + e^{-\tau_{l,2}h} t_n^{-\sigma_2} Y_{n-1}. \tag{37}$$

Theorem 4.2. *Assuming $x = \lambda h$ and $y = \mu^2 h$, the improved stochastic θ-scheme* (34) *can be expressed as follows:*

$$\begin{aligned} Y_{n+1} = \big(A + B\mu\sqrt{h}\eta_n\big) Y_n &+ \theta \sum_{l=1}^{M_{\exp,1}} C_l \tilde{P}_{1,l}(t_n) \\ &+ (1-\theta) \sum_{l=1}^{M_{\exp,1}} C_l \tilde{P}_{2,l}(t_n) + \mu\sqrt{h} \sum_{l=1}^{M_{\exp,2}} D_l \tilde{P}_{3,l}(t_n)\eta_n, \end{aligned} \tag{38}$$

with $Y_1 = \big(A + B\mu\sqrt{h}\eta_0\big)Y_0$ *and*

(39)
$$A = \frac{1 + (1-\theta)x \sum\limits_{l=1}^{M_{\exp,1}} w_{l,1} e^{-\tau_{l,1}h} t_{n+1}^{-\sigma_1}}{1 - \theta x \sum\limits_{l=1}^{M_{\exp,1}} w_{l,1} e^{-\tau_{l,1}h} t_{n+1}^{-\sigma_1}}, \qquad B = \frac{\sum\limits_{l=1}^{M_{\exp,2}} w_{l,2} e^{-\tau_{l,2}h} t_{n+1}^{-\sigma_2}}{1 - \theta x \sum\limits_{l=1}^{M_{\exp,1}} w_{l,1} e^{-\tau_{l,1}h} t_{n+1}^{-\sigma_1}},$$

(40)
$$C_l = \frac{x w_{l,1}(e^{-\tau_{l,1}h} - 1)}{1 - \theta x \sum\limits_{l=1}^{M_{\exp,1}} w_{l,1} e^{-\tau_{l,1}h} t_{n+1}^{-\sigma_1}}, \qquad D_l = \frac{w_{l,2}(e^{-\tau_{l,2}h} - 1)}{1 - \theta x \sum\limits_{l=1}^{M_{\exp,1}} w_{l,1} e^{-\tau_{l,1}h} t_{n+1}^{-\sigma_1}},$$

where $\theta \in [0,1]$ *and* $n = 1, 2, \ldots, N-1$.

Proof. The improved stochastic θ-scheme (34) referred to the point $t = t_{n+1}$ yields:

$$\begin{aligned} Y_{n+1} &= y_0 + \theta\lambda h \sum_{l=1}^{M_{\exp,1}} w_{l,1} \tilde{P}_{1,l}(t_{n+1}) \\ &\quad + (1-\theta)\lambda h \sum_{l=1}^{M_{\exp,1}} w_{l,1} \tilde{P}_{2,l}(t_{n+1}) + \mu\sqrt{h} \sum_{l=1}^{M_{\exp,2}} w_{l,2} \tilde{P}_{3,l}(t_{n+1})\eta_n. \end{aligned} \tag{41}$$

Subtracting Eq. (34) and using the recurrence relations (35)-(37), we obtain:

$$\begin{aligned} Y_{n+1} - Y_n &= \theta\lambda h \sum_{l=1}^{M_{\exp,1}} w_{l,1}\big(\tilde{P}_{1,l}(t_{n+1}) - \tilde{P}_{1,l}(t_n)\big) \\ &\quad + (1-\theta)\lambda h \sum_{l=1}^{M_{\exp,1}} w_{l,1}\big(\tilde{P}_{2,l}(t_{n+1}) - \tilde{P}_{2,l}(t_n)\big) \\ &\quad + \mu\sqrt{h} \sum_{l=1}^{M_{\exp,2}} w_{l,2}\big(\tilde{P}_{3,l}(t_{n+1}) - \tilde{P}_{3,l}(t_n)\big)\eta_n \\ &= \theta\lambda h \sum_{l=1}^{M_{\exp,1}} w_{l,1}\Big(e^{-\tau_{l,1}h} t_{n+1}^{-\sigma_1} Y_{n+1} + e^{-\tau_{l,1}h}\tilde{P}_{1,l}(t_n) - \tilde{P}_{1,l}(t_n)\Big) \\ &\quad + (1-\theta)\lambda h \sum_{l=1}^{M_{\exp,1}} w_{l,1}\Big(e^{-\tau_{l,1}h} t_{n+1}^{-\sigma_1} Y_n + e^{-\tau_{l,1}h}\tilde{P}_{2,l}(t_n) - \tilde{P}_{2,l}(t_n)\Big) \\ &\quad + \mu\sqrt{h} \sum_{l=1}^{M_{\exp,2}} w_{l,2}\Big(e^{-\tau_{l,2}h} t_{n+1}^{-\sigma_2} Y_n + e^{-\tau_{l,2}h}\tilde{P}_{3,l}(t_n) - \tilde{P}_{3,l}(t_n)\Big)\eta_n. \end{aligned} \tag{42}$$

This completes the proof of Theorem 4.2. □

Corollary 4.1. *Let* $C = \big(C_1, C_2, \ldots, C_{M_{\exp,1}}\big)$, $D = \big(D_1, D_2, \ldots, D_{M_{\exp,2}}\big)$, $\tau^* = \big(\tau_{1,1}, \tau_{2,1}, \ldots, \tau_{M_{\exp,1}}\big)$ *and* $\tau^{**} = \big(\tau_{1,2}, \tau_{2,2}, \ldots, \tau_{M_{\exp,2}}\big)$. *Then we have:*

$$\begin{bmatrix} Y_{n+1} \\ \tilde{P}_{1,l}(t_{n+1}) \\ \tilde{P}_{2,l}(t_{n+1}) \\ \tilde{P}_{3,l}(t_{n+1}) \end{bmatrix}$$

$$= \begin{bmatrix} A+B\mu\sqrt{h}\eta_n & \theta C_l & (1-\theta)C_l & \mu\sqrt{h}\eta_n D_l \\ (A+B\mu\sqrt{h}\eta_n)(e^{-\tau_{l,1}h})^T t_{n+1}^{-\sigma_1} & \theta(e^{-\tau_{l,1}h})^T t_{n+1}^{-\sigma_1} C_l + E_1 & (1-\theta)(e^{-\tau_{l,1}h})^T t_{n+1}^{-\sigma_1} C_l & \mu\sqrt{h}\eta_n t_{n+1}^{-\sigma_1} D_l \\ (e^{-\tau_{l,1}h})^T t_{n+1}^{-\sigma_1} & 0 & E_1 & 0 \\ (e^{-\tau_{l,2}h})^T t_{n+1}^{-\sigma_2} & 0 & 0 & E_2 \end{bmatrix}$$

$$\times \begin{bmatrix} Y_n \\ \tilde{P}_{1,l}(t_n) \\ \tilde{P}_{2,l}(t_n) \\ \tilde{P}_{3,l}(t_n) \end{bmatrix}$$

$$:= H\left[Y_n, \tilde{P}_{1,l}(t_n), \tilde{P}_{2,l}(t_n), \tilde{P}_{3,l}(t_n)\right]^T, \tag{43}$$

where $\tilde{P}_{i,l}(t_n) = \big[\tilde{P}_{i,1}(t_n), \tilde{P}_{i,2}(t_n), \ldots, \tilde{P}_{i,M_{\exp}}(t_n)\big]^T$ $(i = 1, 2, 3)$ *is an* $M_{\exp} \times 1$ *column vector. Additionally,* E_1 *and* E_2 *are diagonal matrices as follows:*

$$E_1 = \exp(-\tau^* h) I_{M_{\exp,1}} = \begin{bmatrix} e^{-\tau_{1,1}h} & & & \\ & e^{-\tau_{2,1}h} & & \\ & & \ddots & \\ & & & e^{-\tau_{M_{\exp,1}}h} \end{bmatrix}, \tag{44}$$

$$E_2 = \exp(-\tau^{**} h) I_{M_{\exp,2}} = \begin{bmatrix} e^{-\tau_{1,2}h} & & & \\ & e^{-\tau_{2,2}h} & & \\ & & \ddots & \\ & & & e^{-\tau_{M_{\exp,2}}h} \end{bmatrix}, \tag{45}$$

where $I_{M_{\exp,1}}$ *and* $I_{M_{\exp,2}}$ *are both identity matrices.*

By Corollary 4.1, one can readily present the following recurrence relations. These relations emphasize a useful attribute for deriving the stability matrix of the improved θ-scheme (34).

Lemma 4.2. *For the improved* θ*-scheme* (34)*, we have:*

$$\mathbb{E}\Big(\big(A + B\sqrt{y}\eta_n\big)Y_n Y_{n+1}\Big) = \big(A^2 + B^2 y\big)\mathbb{E}\big(Y_n^2\big) + A\theta \sum_{l=1}^{M_{\exp,1}} C_l \mathbb{E}\big(Y_n \tilde{P}_{1,l}(t_n)\big)$$

$$+ A(1-\theta) \sum_{l=1}^{M_{\exp,1}} C_l \mathbb{E}\big(Y_n \tilde{P}_{2,l}(t_n)\big) + By \sum_{l=1}^{M_{\exp,2}} D_l \mathbb{E}\big(Y_n \tilde{P}_{3,l}(t_n)\big), \tag{46}$$

and

$$\mathbb{E}\Big(\tilde{P}_{i,j}(t_n) Y_{n+1}\Big) = A\mathbb{E}\Big(\tilde{P}_{i,j}(t_n) Y_n\Big) + \theta \sum_{l=1}^{M_{\exp,1}} C_l \mathbb{E}\Big(\tilde{P}_{i,j}(t_n)\tilde{P}_{1,l}(t_n)\Big)$$

$$+ (1-\theta) \sum_{l=1}^{M_{\exp,1}} C_l \mathbb{E}\Big(\tilde{P}_{i,j}(t_n)\tilde{P}_{2,l}(t_n)\Big), \quad i = 1, 2, 3,\ j = 1, 2, \cdots, M_{\exp,1}. \tag{47}$$

Proof. Multiplying Eq. (38) by $\big(A + B\sqrt{y}\eta_n\big)Y_n$ and $\tilde{P}_{i,j}(t_n)$, we deduce:

$$\begin{aligned}\big(A + B\sqrt{y}\eta_n\big)Y_nY_{n+1} &= \big(A + B\sqrt{y}\eta_n\big)^2Y_n^2 + \big(A + B\sqrt{y}\eta_n\big)\theta \sum_{l=1}^{M_{\exp,1}} C_l\tilde{P}_{1,l}(t_n)Y_n \\ &\quad + \big(A + B\sqrt{y}\eta_n\big)(1-\theta) \sum_{l=1}^{M_{\exp,1}} C_l\tilde{P}_{2,l}(t_n)Y_n \\ &\quad + \big(A + B\sqrt{y}\eta_n\big)\sqrt{y}\eta_n \sum_{l=1}^{M_{\exp,2}} D_l\tilde{P}_{3,l}(t_n)Y_n, \end{aligned} \tag{48}$$

and

$$\begin{aligned}\tilde{P}_{i,j}(t_n)Y_{n+1} &= \big(A + B\sqrt{y}\eta_n\big)\tilde{P}_{i,j}(t_n)Y_n + \theta \sum_{l=1}^{M_{\exp,1}} C_l\tilde{P}_{i,j}(t_n)\tilde{P}_{1,l}(t_n) \\ &\quad + (1-\theta) \sum_{l=1}^{M_{\exp,1}} C_l\tilde{P}_{i,j}(t_n)\tilde{P}_{2,l}(t_n) + \sqrt{y}\eta_n \sum_{l=1}^{M_{\exp,2}} D_l\tilde{P}_{i,j}(t_n)\tilde{P}_{3,l}(t_n). \end{aligned} \tag{49}$$

Therefore, by employing the expectations on both sides, we obtain the relationships expressed in (46) and (47). □

We now turn to scheme (34) obtained by applying the stochastic θ-scheme to test Eq. (16). We rewrite each of these stochastic difference equations into an explicit one-step recurrence equation involving a sequence $\{H_n\}_{n\geq 1}$ of independent random matrices:

$$Y_{n+1} = H_nY_n, \quad n = 1, \ldots, N-1. \tag{50}$$

The entries of the matrix H_n depend on entries of the drift and diffusion matrices of test Eq. (16) as well as on the parameter θ of the scheme and the applied step size h. For each $n \in \mathbb{N}_0$ the matrix H_n also depends on the random variables η_n. To obtain the second moments of the discrete approximation process Y_n, we multiply each side of Eq. (50) by Y_{n+1}^T and $(H_nY_n)^T$, respectively, and take expectations. Then applying the vectorisation operation to both sides yields:

$$\mathbb{E}(Z_{n+1}) = \mathbb{E}(H_n \otimes H_n)\mathbb{E}(Z_n), \tag{51}$$

where the d^2-dimensional discrete process Z_n is given by $Z_n = vec(Y_nY_n^T)$. We set:

$$\mathcal{S} = \mathbb{E}(H \otimes H), \tag{52}$$

and refer to $\mathcal{S}$ as the mean square stability matrix of the numerical scheme. The following result is originally due to Bellman [34], but can also be found in [2, 27].

Lemma 4.3. *The zero solution of the system* (50) *is asymptotically stable in mean square if and only if:*

$$\rho(\mathcal{S}) < 1. \tag{53}$$

Remark 4.1. *We have omitted the index of the matrices H in* (52)*, as the sequence $\{H_n\}$ is i.i.d. This notation is consistent with the one used in* [34].

Theorem 4.3. *The improved θ-scheme* (34) *for evaluating the test Eq.* (16) *with double singular kernels exhibits mean square stability if the spectral radius*

$\rho\big(\mathbb{E}(H\otimes H)\big)<1$, *where*

$$\mathbb{E}\big(H\otimes H\big)$$

(54)

$$=\begin{bmatrix} U & \theta(C_l\otimes V) & (1-\theta)(C_l\otimes V) & (ByD_l)\otimes V \\ t_{n+1}^{-\sigma_1}(e^{-\tau_{l,1}h})^T\otimes U & (\theta(e^{-\tau_{l,1}h})^T t_{n+1}^{-\sigma_1}C_l+E_1\otimes V & ((1-\theta)(e^{-\tau_{l,1}h})^T t_{n+1}^{-\sigma_1}C_l)\otimes V & (Byt_{n+1}^{-\beta_1}D_l)\otimes V \\ ((e^{-\tau_{l,1}h})^T t_{n+1}^{-\sigma_1\sigma}\otimes V & 0 & E_1\otimes V & 0 \\ ((e^{-\tau_{l,2}h})^T t_{n+1}^{-\sigma_2})\otimes V & 0 & 0 & E_2\otimes V \end{bmatrix}.$$

Here, the symbol $\otimes$ *represents the Kronecker product and*

(55)

$$U=\begin{bmatrix} A^2+B^2y & A\theta C_l & A(1-\theta)C_l & ByD_l \\ (A^2+B^2y)(e^{-\tau_{l,1}h})^T t_{n+1}^{-\sigma_1} & A\theta(e^{-\tau_{l,1}h})^T t_{n+1}^{-\sigma_1}C_l+AE_1 & A(1-\theta)(e^{-\tau_{l,1}h})^T t_{n+1}^{-\sigma_1}C_l & Byt_{n+1}^{-\sigma_1}D_l \\ A(e^{-\tau_{l,1}h})^T t_{n+1}^{-\sigma_1} & 0 & AE_1 & 0 \\ A(e^{-\tau_{l,2}h})^T t_{n+1}^{-\sigma_2} & 0 & 0 & AE_2 \end{bmatrix},$$

(56)

$$V=\begin{bmatrix} A & \theta C_l & (1-\theta)C_l & 0 \\ A(e^{-\tau_{l,1}h})^T t_{n+1}^{-\sigma_1} & \theta(e^{-\tau_{l,1}h})^T t_{n+1}^{-\sigma_1}C_l+E_1 & (1-\theta)(e^{-\tau_{l,1}h})^T t_{n+1}^{-\sigma_1}C_l & 0 \\ (e^{-\tau_{l,1}h})^T t_{n+1}^{-\sigma_1} & 0 & E_1 & 0 \\ (e^{-\tau_{l,2}h})^T t_{n+1}^{-\sigma_2} & 0 & 0 & E_2 \end{bmatrix}.$$

Proof. By Lemma 4.2, we get the following result:

$$\begin{aligned}\mathbb{E}\big(Y_{n+1}Y_{n+1}\big) &= \big(A^2+B^2y\big)\mathbb{E}\big(Y_n^2\big)+A\theta\sum_{l=1}^{M_{\exp,1}} C_l\mathbb{E}\big(Y_n\tilde{P}_{1,l}(t_n)\big)\\ &\quad+A(1-\theta)\sum_{l=1}^{M_{\exp,1}} C_l\mathbb{E}\big(Y_n\tilde{P}_{2,l}(t_n)\big)+By\sum_{l=1}^{M_{\exp,2}} D_l\mathbb{E}\big(Y_n\tilde{P}_{3,l}(t_n)\big)\\ &\quad+\theta\sum_{l=1}^{M_{\exp,1}} C_l\Big(A\mathbb{E}\big(Y_n\tilde{P}_{1,l}(t_n)\big)+\theta\sum_{i=1}^{M_{\exp,1}} C_i\mathbb{E}\big(\tilde{P}_{1,l}(t_n)\tilde{P}_{1,i}(t_n)\big)\\ &\quad+(1-\theta)\sum_{i=1}^{M_{\exp,1}} C_i\mathbb{E}\big(\tilde{P}_{1,l}(t_n)\tilde{P}_{2,i}(t_n)\big)\Big)+(1-\theta)\sum_{l=1}^{M_{\exp,1}} C_l\Big(A\mathbb{E}\big(Y_n\tilde{P}_{2,l}(t_n)\big)\\ &\quad+\theta\sum_{i=1}^{M_{\exp,1}} C_i\mathbb{E}\big(\tilde{P}_{2,l}(t_n)\tilde{P}_{1,i}(t_n)\big)+(1-\theta)\sum_{i=1}^{M_{\exp,1}} C_i\mathbb{E}\big(\tilde{P}_{2,l}(t_n)\tilde{P}_{2,i}(t_n)\big)\Big)\\ &\quad+\sum_{l=1}^{M_{\exp,2}} D_l\Big(By\mathbb{E}\big(Y_n\tilde{P}_{3,l}(t_n)\big)+y\sum_{i=1}^{M_{\exp,2}} D_i\mathbb{E}\big(\tilde{P}_{3,l}(t_n)\tilde{P}_{3,i}(t_n)\big)\Big). \qquad (57)\end{aligned}$$

Following a similar approach yields:

$$\begin{aligned}&\mathbb{E}\big(\tilde{P}_{1,j}(t_{n+1})\tilde{P}_{2,m}(t_{n+1})\big)\\ &=Ae^{-(\tau_{j,1}+\tau_{m,1})h}t_{n+1}^{-2\sigma_1}\mathbb{E}\big(Y_n^2\big)+Ae^{-(\tau_{j,1}+\tau_{m,1})h}t_{n+1}^{-\sigma_1}\mathbb{E}\big(Y_n\tilde{P}_{2,m}(t_n)\big)\\ &\quad+\theta e^{-(\tau_{j,1}+\tau_{m,1})h}\sum_{i=1}^{M_{\exp,1}} C_i\Big(t_{n+1}^{-2\sigma_1}\mathbb{E}\big(Y_n\tilde{P}_{1,i}(t_n)\big)+t_{n+1}^{-\sigma_1}\mathbb{E}\big(\tilde{P}_{2,m}(t_n)\tilde{P}_{1,i}(t_n)\big)\Big)\\ &\quad+(1-\theta)e^{-(\tau_{j,1}+\tau_{m,1})h}\sum_{i=1}^{M_{\exp,1}} C_i\Big(t_{n+1}^{-2\sigma_1}\mathbb{E}\big(Y_n\tilde{P}_{2,i}(t_n)\big)+t_{n+1}^{-\sigma_1}\mathbb{E}\big(\tilde{P}_{2,j}(t_n)\tilde{P}_{2,i}(t_n)\big)\Big) \qquad (58)\\ &\quad+e^{-(\tau_{j,1}+\tau_{m,1})h}\Big(t_{n+1}^{-\sigma_1}\mathbb{E}\big(Y_n\tilde{P}_{1,j}(t_n)\big)+\mathbb{E}\big(\tilde{P}_{2,m}(t_n)\tilde{P}_{1,i}(t_n)\big)\Big),\end{aligned}$$

$$
\begin{aligned}
&\mathbb{E}\big(\tilde{P}_{1,j}(t_{n+1})\tilde{P}_{3,r}(t_{n+1})\big)\\
=&Ae^{-(\tau_{j,1}+\tau_{r,2})h}t_{n+1}^{-(\sigma_1+\sigma_2)}\mathbb{E}\big(Y_n^2\big)+Ae^{-(\tau_{j,1}+\tau_{r,2})h}t_{n+1}^{-\sigma_1}\mathbb{E}\big(Y_n\tilde{P}_{3,r}(t_n)\big)\\
&+\theta e^{-(\tau_{j,1}+\tau_{r,2})h}\sum_{i=1}^{M_{\exp,1}}C_i\Big(t_{n+1}^{-(\sigma_1+\sigma_2)}\mathbb{E}\big(Y_n\tilde{P}_{1,i}(t_n)\big)+t_{n+1}^{-\sigma_1}\mathbb{E}\big(\tilde{P}_{3,r}(t_n)\tilde{P}_{1,i}(t_n)\big)\Big)\\
&+(1-\theta)e^{-(\tau_{j,1}+\tau_{r,2})h}\sum_{i=1}^{M_{\exp,1}}C_i\Big(t_{n+1}^{-(\sigma_1+\sigma_2)}\mathbb{E}\big(Y_n\tilde{P}_{2,i}(t_n)\big)+t_{n+1}^{-\sigma_1}\mathbb{E}\big(\tilde{P}_{3,r}(t_n)\tilde{P}_{2,i}(t_n)\big)\Big)\\
&+e^{-(\tau_{j,1}+\tau_{r,2})h}\Big(t_{n+1}^{-\sigma_2}\mathbb{E}\big(Y_n\tilde{P}_{1,j}(t_n)\big)+\mathbb{E}\big(\tilde{P}_{3,r}(t_n)\tilde{P}_{1,j}(t_n)\big)\Big),
\end{aligned}
\tag{59}
$$

and

$$
\begin{aligned}
&\mathbb{E}\big(\tilde{P}_{2,m}(t_{n+1})\tilde{P}_{3,r}(t_{n+1})\big)\\
=&e^{-(\tau_{m,1}+\tau_{r,2})h}t_{n+1}^{-(\sigma_1+\sigma_2)}\mathbb{E}\big(Y_n^2\big)+e^{-(\tau_{m,1}+\tau_{r,2})h}t_{n+1}^{-\sigma_1}\mathbb{E}\big(Y_n\tilde{P}_{3,r}(t_n)\big)\\
&+e^{-(\tau_{m,1}+\tau_{r,2})h}t_{n+1}^{-\sigma_2}\mathbb{E}\big(Y_n\tilde{P}_{2,m}(t_n)\big)+e^{-(\tau_{m,1}+\tau_{r,2})h}\mathbb{E}\big(\tilde{P}_{2,m}(t_n)\tilde{P}_{3,r}(t_n)\big),
\end{aligned}
\tag{60}
$$

where $j,m,r=1,2,\cdots,M_{\exp,1}$. Now we set:

$$
\begin{aligned}
Z_{n+1}:=\Big[&Y_{n+1}^2,Y_{n+1}\tilde{P}_{1,l}(t_{n+1}),Y_{n+1}\tilde{P}_{2,l}(t_{n+1}),Y_{n+1}\tilde{P}_{3,l}(t_{n+1}),\tilde{P}_{1,l}(t_{n+1})Y_{n+1},\\
&\tilde{P}_{1,l}^2(t_{n+1}),\tilde{P}_{1,l}(t_{n+1})\tilde{P}_{2,l}(t_{n+1}),\tilde{P}_{1,l}(t_{n+1})\tilde{P}_{3,l}(t_{n+1}),\tilde{P}_{2,l}(t_{n+1})Y_{n+1},\\
&\tilde{P}_{2,l}(t_{n+1})\tilde{P}_{1,l}(t_{n+1}),\tilde{P}_{2,l}^2(t_{n+1}),\tilde{P}_{2,l}(t_{n+1})\tilde{P}_{3,l}(t_{n+1}),\tilde{P}_{3,l}(t_{n+1})Y_{n+1},\\
&\tilde{P}_{3,l}(t_{n+1})\tilde{P}_{1,l}(t_{n+1}),\tilde{P}_{3,l}(t_{n+1})\tilde{P}_{2,l}(t_{n+1}),\tilde{P}_{3,l}^2(t_{n+1})\Big]^T.
\end{aligned}
\tag{61}
$$

Then, based on Eq.s (57)-(60), we have:

$$
\mathbb{E}\big(Z_{n+1}\big)=\mathbb{E}\big(H\otimes H\big)\mathbb{E}\big(Z_n\big). \tag{62}
$$

When the spectral radius $\rho\big(\mathbb{E}(H\otimes H)\big)<1$, the proposed scheme is mean square stable. □

5. Numerical experiments

The objective of this section is to present two examples to illustrate our numerical stability results of proposed scheme through a comparison with the split-step θ-method [4] and the θ-Milstein method [12], using the SOE approximation.

Example 5.1. *Let us consider the following double singular test equation:*

$$
y(t)=y_0+\lambda\int_0^t(t-s)^{-\gamma_1}s^{-\sigma_1}y(s)ds+\mu\int_0^t(t-s)^{-\gamma_2}s^{-\sigma_2}y(s)dW(s),\quad t\in[0,T], \tag{63}
$$

where $\gamma_1+\sigma_1\in(0,1)$ *and* $\gamma_2+\sigma_2\in(0,\frac{1}{2})$. *To report our stability regions for different values of* θ, *we use the following three cases:*

- *Case I:* $\gamma_1=0.2$, $\sigma_1=0.1$, $\gamma_2=0.2$, $\sigma_2=0.1$ *and* $h=2^{-6}$,
- *Case II:* $\gamma_1=0.2$, $\sigma_1=0.1$, $\gamma_2=0.2$, $\sigma_2=0.1$ *and* $h=2^{-10}$,
- *Case III:* $\gamma_1=0.4$, $\sigma_1=0.3$, $\gamma_2=0.2$, $\sigma_2=0.1$ *and* $h=2^{-10}$.

Following [11] *regarding the scaling of the parameters in the plots, we now set:*

$$
x:=\lambda h,\quad y:=\mu^2 h,\quad \textit{and}\ \ T=25.
$$

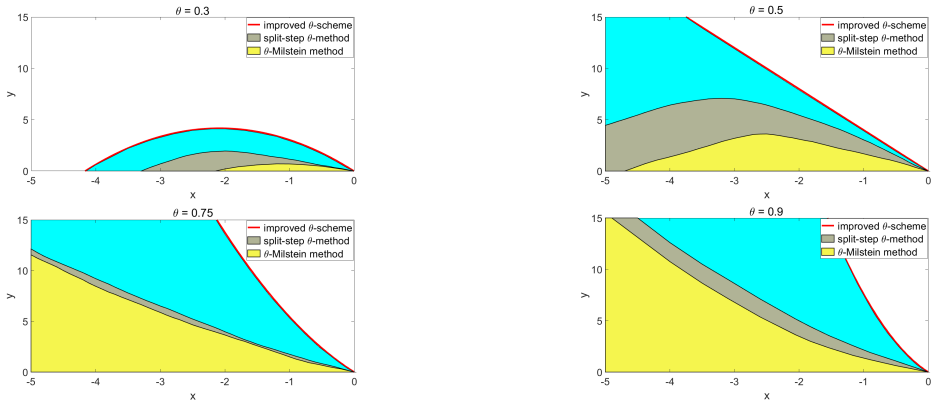

FIGURE 1. Boundaries of the mean square stability regions in the (x, y)-plane for the proposed scheme (cyan area), the split-step θ-method (grey area) and the θ-Milstein method (yellow area) with $h = 2^{-6}$ for case I.

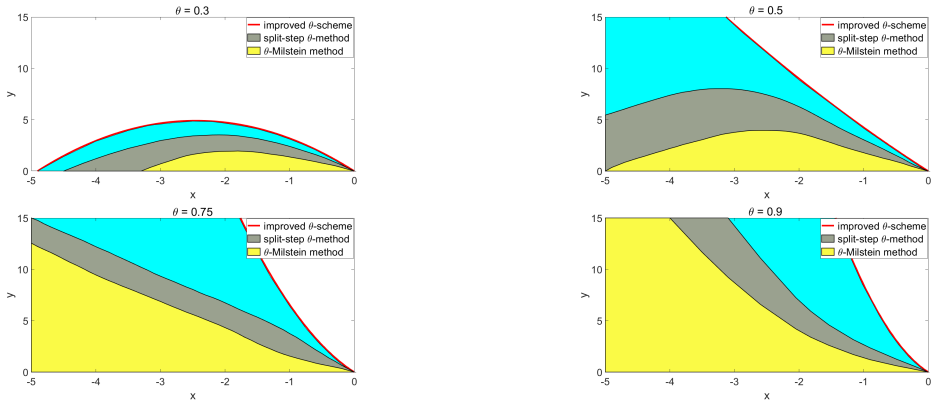

FIGURE 2. Boundaries of the mean square stability regions in the (x, y)-plane for the proposed scheme (cyan area), the split-step θ-method (grey area) and the θ-Milstein method (yellow area) with $h = 2^{-10}$ for case II.

The stability results of the three cases with different kernel parameters are shown in Figs. 1-3. When the values of θ increase, Figs. 1 and 2 illustrate that the stability regions of the proposed scheme is expanded significantly. In particular, in Fig. 3, we can see that as the kernel parameters increase and other quantities are unchanged, the stability regions of the proposed scheme will become large.

Firstly, we test for different values of θ and step sizes $h = 2^{-6}$ and $h = 2^{-10}$, respectively, and their stability regions in the (x, y)-plane are given in Figs. 1 and 2. For the given test Eq. (63) *with the kernel parameters introduced in case I, we select $\lambda = -3$, $\mu = 2$, and five different step sizes $h = 1, 2^{-1}, 2^{-2}, 2^{-4}$ and 2^{-6}. Using these values, we generate 10^4 numerical sample paths over the interval $[0, 25]$ and plot the mean square of the numerical solution in Fig. 4, which indicates that the numerical scheme tends to be stable as the step size decreases. Further, we test the proposed scheme with step size $h = 2^{-6}$ for the test Eq.* (63) *with $\lambda = -85$,*

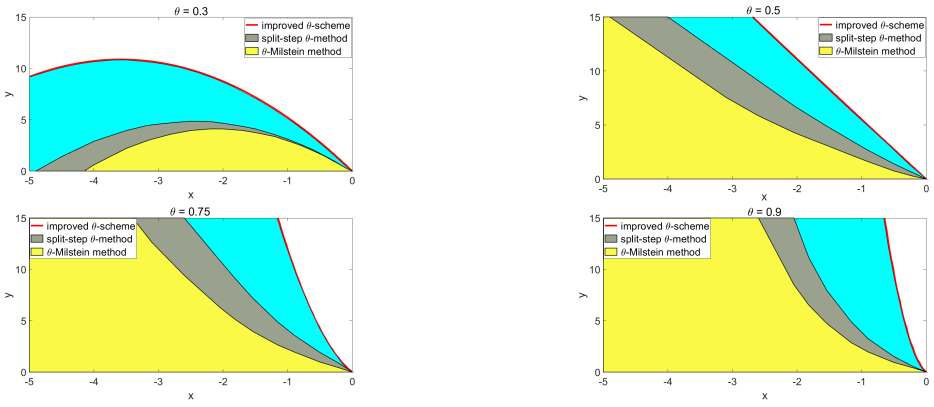

FIGURE 3. Boundaries of the mean square stability regions in the (x, y)-plane for the proposed scheme (cyan area), the split-step θ-method (grey area) and the θ-Milstein method (yellow area) with $h = 2^{-10}$ for case III.

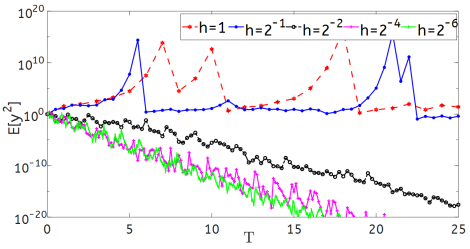

FIGURE 4. Mean square of the numerical solution of the proposed scheme for the test Eq. (63) with $\lambda = -3$, $\mu = 2$ and $\theta = 0.3$.

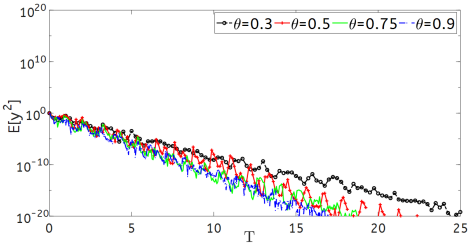

FIGURE 5. Mean square of the numerical solution of the proposed scheme for the test Eq. (63) with $\lambda = -85$, $\mu = 2$ and $h = 2^{-6}$.

$\mu = 2$, and different values of θ so that the point $(x, y) = (-1.3281, 0.0625)$ lies inside the stability region. The mean square of the numerical solution is plotted in Fig. 5, demonstrating stability for all values of θ. Next, we make a comparison between the stability of the proposed scheme and that of the split-step θ-method and θ-Milstein method. We take $\theta = 0.5$ and consider the test Eq. (63) with $\lambda = -8$ and $\mu = 4$. For $h = 2^{-1}$, the numerical results are depicted in Fig. 6, which shows that the proposed scheme is stable while the split-step θ-method and θ-Milstein method are unstable. This is because the corresponding point $(x, y) = (-4, 8)$ lies inside the

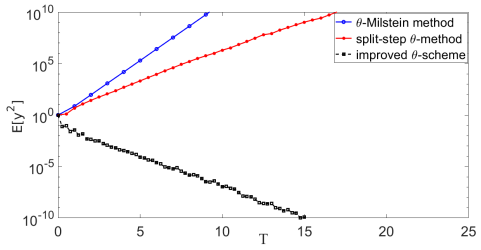

FIGURE 6. Mean square of the numerical solutions of three methods for the test Eq. (63) with $\theta = 0.5$, $\lambda = -8$, $\mu = 4$ and step size $h = 2^{-1}$.

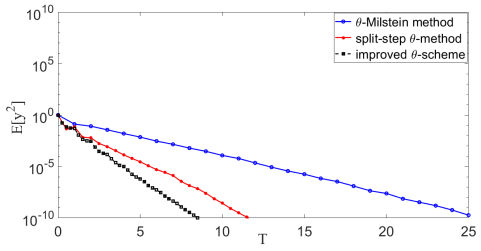

FIGURE 7. Mean square of the numerical solutions of three methods for the test Eq. (63) with $\theta = 0.5$, $\lambda = -8$, $\mu = 4$ and step size $h = 2^{-6}$.

stability region of the proposed scheme, but outside that of the split-step θ-method and θ-Milstein method. If we reduce the step size to $h = 2^{-6}$, then three methods are mean square stable, which is shown in Fig. 7. This shows that the stability of the θ-Milstein method and the split-step θ-method are less restrictive than that of the improved stochastic θ-scheme. As a further aspect of providing comparisons of the stability properties of the methods, we now consider a fixed set of values of the parameters λ and μ and, using Matlab, *numerically evaluate the spectral radius of the stability matrices $H \otimes H$ for different values of step sizes h and parameter θ. Table 1 provide the corresponding values and illustrate clearly the different stability properties of the three methods considered.*

Example 5.2. *Let us consider the following nonlinear singular SVIE with Mittag-Leffler kernels:*

$$y(t) = y_0 + \lambda \int_0^t (t-s)^{-\gamma} E_\alpha\big((t-s)^\alpha\big) \sin(y(s)) ds + \mu \int_0^t (t-s)^{-\sigma} E_\alpha\big((t-s)^\alpha\big) \cos(y(s)) dW(s), \quad t \in [0,T], \tag{64}$$

where $\gamma \in (0,1)$, $\sigma \in (0, \frac{1}{2})$ and $\alpha \in (0,1)$. It is obvious that the coefficients F and G satisfy the global Lipschitz condition and linear growth condition. Next, we will give the stability results of the proposed scheme for the nonlinear test Eq. (64) with $\gamma = 0.6$, $\sigma = 0.3$ and $\alpha = 0.9$.

TABLE 1. Values of the spectral radius of the stability matrices $H \otimes H$ for the test Eq. (63) with $\lambda = -3$ and $\mu = 2$.

		Improved θ-scheme			*Split-step θ-method*			*θ-Milstein method*		
	h	$\theta = 0.3$	$\theta = 0.5$	$\theta = 0.9$	$\theta = 0.3$	$\theta = 0.5$	$\theta = 0.9$	$\theta = 0.3$	$\theta = 0.5$	$\theta = 0.9$
Case I	2^{-1}	*3.857 unst.*	*0.737 stable*	*0.518 stable*	*6.420 unst.*	*2.917 unst.*	*0.354 stable*	*15.33 unst.*	*5.509 unst.*	*3.841 unst.*
	2^{-2}	*0.894 stable*	*0.843 stable*	*0.649 stable*	*1.284 unst.*	*0.744 stable*	*0.562 stable*	*2.901 unst.*	*1.438 unst.*	*0.731 stable*
	2^{-4}	*0.924 stable*	*0.871 stable*	*0.735 stable*	*0.873 stable*	*0.796 stable*	*0.691 stable*	*1.12 unst.*	*0.726 stable*	*0.856 stable*
	2^{-6}	*0.941 stable*	*0.917 stable*	*0.820 stable*	*0.904 stable*	*0.835 stable*	*0.805 stable*	*0.762 stable*	*0.794 stable*	*0.927 stable*
	2^{-10}	*0.987 stable*	*0.952 stable*	*0.936 stable*	*0.926 stable*	*0.891 stable*	*0.836 stable*	*0.803 stable*	*0.907 stable*	*0.935 stable*
Case III	2^{-1}	*0.876 stable*	*0.851 stable*	*0.828 stable*	*3.677 unst.*	*0.539 stable*	*0.513 stable*	*5.449 unst.*	*3.175 unst.*	*1.545 unst.*
	2^{-2}	*0.931 stable*	*0.887 stable*	*0.843 stable*	*1.056 unst.*	*0.574 stable*	*0.549 stable*	*1.156 unst.*	*1.004 unst.*	*0.452 stable*
	2^{-4}	*0.958 stable*	*0.922 stable*	*0.895 stable*	*0.670 stable*	*0.638 stable*	*0.606 stable*	*0.526 stable*	*0.508 stable*	*0.496 stable*
	2^{-6}	*0.975 stable*	*0.967 stable*	*0.942 stable*	*0.782 stable*	*0.715 stable*	*0.709 stable*	*0.717 stable*	*0.643 stable*	*0.630 stable*
	2^{-10}	*0.992 stable*	*0.980 stable*	*0.971 stable*	*0.954 stable*	*0.921 stable*	*0.851 stable*	*0.845 stable*	*0.837 stable*	*0.826 stable*

FIGURE 8. Boundaries of the mean square stability regions in the (x, y)-plane for the proposed scheme (cyan area), the split-step θ-method (grey area) and the θ-Milstein method (yellow area) with step size $h = 2^{-6}$.

FIGURE 9. Boundaries of the mean square stability regions in the (x, y)-plane for the proposed scheme (cyan area), the split-step θ-method (grey area) and the θ-Milstein method (yellow area) with step size $h = 2^{-10}$.

Now, we verify the numerical stability results given in Figs. 8 and 9. Firstly, we test for two values of θ *and step sizes* $h = 2^{-6}$ *and* 2^{-10}*, respectively, and their stability regions in the* (x, y)*-plane. Figs. 8 and 9 show that the stability regions of the proposed scheme become large when the value of* θ *increases. For the given nonlinear test Eq.* (64)*, we generate* 10^4 *numerical sample paths over the interval* $[0, 25]$ *and plot the mean square of the numerical solution, which indicates that the numerical scheme tends to be stable as the step size decreases.*

Next, we make a comparison between the stability of the proposed scheme and that of the split-step θ*-method and* θ*-Milstein method. We take* $\theta = 0.5$ *and consider the nonlinear test Eq.* (64) *with* $\lambda = -150$ *and* $\mu = 12$*. For* $h = 2^{-6}$*, the numerical results are depicted in Fig. 10, which shows that the proposed scheme is stable while the split-step* θ*-method and* θ*-Milstein method are unstable. This is because the corresponding point* $(x, y) = (-2.34, 2.25)$ *lies inside the stability region of the proposed scheme, but outside that of the split-step* θ*-method and* θ*-Milstein method. If we reduce the step size to* $h = 2^{-10}$*, then three methods are mean square stable, which is shown in Fig. 11. This shows that the stability of the* θ*-Milstein method and the split-step* θ*-method are less restrictive than that of the proposed scheme. Table 2 provide the corresponding values and illustrate clearly the different stability properties of the three methods considered.*

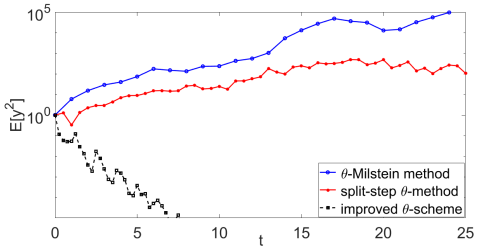

FIGURE 10. Mean square of the numerical solutions of three methods for the nonlinear test Eq. (64) with $\theta = 0.5$, $\lambda = -150$, $\mu = 12$ and step size $h = 2^{-6}$.

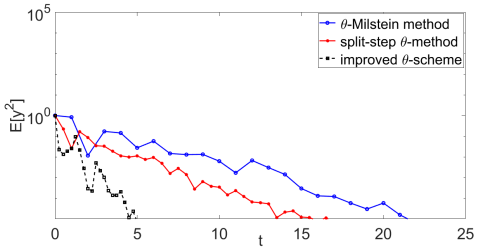

FIGURE 11. Mean square of the numerical solutions of three methods for the nonlinear test Eq. (64) with $\theta = 0.5$, $\lambda = -150$, $\mu = 12$ and step size $h = 2^{-10}$.

TABLE 2. Values of the spectral radius of the stability matrices $H \otimes H$ for the nonlinear test Eq. (64) with $\lambda = -150$ and $\mu = 12$.

	Improved θ-scheme		*Split-step θ-method*		*θ-Milstein method*	
h	$\theta = 0.5$	$\theta = 0.8$	$\theta = 0.5$	$\theta = 0.8$	$\theta = 0.5$	$\theta = 0.8$
2^{-1}	*0.675 stable*	*0.591 stable*	*1.944 unst.*	*0.468 stable*	*3.511 unst.*	*2.099 unst.*
2^{-2}	*0.706 stable*	*0.636 stable*	*0.551 stable*	*0.533 stable*	*1.244 unst.*	*0.410 stable*
2^{-4}	*0.759 stable*	*0.702 stable*	*0.617 stable*	*0.582 stable*	*0.528 stable*	*0.473 stable*
2^{-6}	*0.821 stable*	*0.778 stable*	*0.683 stable*	*0.645 stable*	*0.574 stable*	*0.533 stable*
2^{-10}	*0.934 stable*	*0.854 stable*	*0.746 stable*	*0.707 stable*	*0.645 stable*	*0.607 stable*

6. Conclusion

This paper presents an innovative method for constructing the stochastic θ-scheme for SVIEs (1) with double singular kernels. The proposed approach utilizes the SOE approximation to improve computational efficiency. Furthermore, we discussed an analysis on the mean square stability of the proposed scheme, focusing specifically on a linear test equation. Based on the explicit structure of the stability matrices, we plotted and compared the numerical stability regions.

Acknowledgments

The first author is supported by a research postdoctoral grant of University of Tabriz (No. 940).

Funding

The authors declare that no funds, grants, or other support were received during the preparation of this manuscript.

Data availability

Data sharing not applicable to this article as no data sets were generated or analyzed during the current study.

References

[1] O. Farkhondeh Rouz, S. Shahmorad, and D. Ahmadian, Double weakly singular kernels in stochastic Volterra integral equations with application to the rough Heston model, Appl. Math. Comput., 475 (2024), 128720.
[2] R. Khasminskii, Stochastic stability of differential equations, Springer, Berlin, (2012).
[3] N. Agram and B. Oksendal, Malliavin calculus and optimal control of stochastic Volterra equations, J. Optim. Theory Appl., 167 (2015), 1070–1094.
[4] M. Li, C. Huang, P. Hu, and J. Wen, Mean-square stability and convergence of a split-step theta method for stochastic Volterra integral equations, J. Comput. Appl. Math., 382 (2021), Article ID 13077.
[5] Y. Li, W. Song, Y. Jiang, and A. Kudreyko, Galerkin approximation for stochastic Volterra integral equations with doubly singular kernels, Fractal Fract., 6 (2022), 1–12.
[6] Y. Xiao, J. Shi, and Z. Yang, Split-step collocation methods for stochastic Volterra integral equations, J. Integral Equ. Appl., 30 (2018), 197–218.
[7] S. Jiang, J. Zhang, Q. Zhang, and et al., Fast evaluation of the Caputo fractional derivative and its applications to fractional diffusion equations, Commun. Comput. Phys., 21 (2017), 650–678.
[8] C.P. Tsokos and W.J. Padgett, Random Integral Equations with Applications to Life Sciences and Engineering, Academic Press, (1974).
[9] S. Vahdati, A wavelet method for stochastic Volterra integral equations and its application to general stock model, Comput. Methods Differ. Equ., 5 (2017), 170–188.
[10] S. Wang, S. Jiang, and J. Wang, Fast high-order integral equation methods for solving boundary value problems of two dimensional heat equation in complex geometry, J. Sci. Comput., 79 (2019), 787–808.
[11] D.J. Higham, Mean-square and asymptotic stability of the stochastic theta method, SIAM J. Numer. Anal., 38 (2000), 753–769.
[12] E. Buckwar and T. Sickenberger, A structural analysis of asymptotic mean-square stability for multi-dimensional linear stochastic differential systems, Appl. Numer. Math., 62 (2012), 842–859.
[13] Q. Zhao, R. Wang, and R. Wei, Exponential utility maximization for an insurer with time-inconsistent preferences, Insur.: Math. Econ., 70 (2016), 89–104.
[14] I. Podlubny, Fractional differential equations. An introduction to fractional derivatives, fractional differential equations, to methods of their solution and some of their applications, Academic Press, Inc, San Diego, CA., (1999), 1–36.
[15] D. Szynal and S. Wedrychowicz, On solutions of a stochastic integral equation of the Volterra type with applications for chemotherapy, J. Appl. Probab., 25 (1988), 257–267.
[16] M. Berger and V. Mizel, Volterra equations with Itô integrals-I, J. Int. Equ., 2 (1980), 187–245.
[17] M. Berger and V. Mizel, Volterra equations with Itô integrals II, J. Int. Equ., 2 (1980), 319–337.
[18] X. Mao, Stochastic Differential Equations and Applications, Horwood Publishing, Chichester, (2008).
[19] M. Li, C. Huang, and Y. Hu, Numerical methods for stochastic Volterra integral equations with weakly singular kernels, IMA J. Numer. Anal., 42 (2022), 2656–2683.
[20] M. Wang, X. Dai, Y. Yu, and A. Xiao, Fast θ-Maruyama scheme for stochastic Volterra integral equations of convolution type: mean-square stability and strong convergence analysis, Comput. Appl. Math., 42 (2023), 1–36.
[21] Y. Yan, Z.Z. Sun, and J. Zhang, Fast evaluation of the Caputo fractional derivative and its applications to fractional diffusion equations: a second-order scheme, Commun. Comput. Phys., 22 (2017), 1028–1048.

[22] P.T. Anh, T.S. Doan and P.T. Huong, A variation of constant formula for Caputo fractional stochastic differential equations, Statist. Probab. Lett., 145 (2019), 351–358.
[23] D. Conte, R. D'Ambrosio, and B. Paternoster, On the stability of θ-methods for stochastic Volterra integral equations, Discrete Contin. Dyn. Syst. Ser B., 23 (2018), 2695–2708.
[24] D. Conte, R. D'Ambrosio, and B. Paternoster, Improved θ-methods for stochastic Volterra integral equations, Commun. Nonlinear Sci. Numer. Simulat., 93 (2021), 105528.
[25] H. Liang, Z. Yang, and J. Gao, Strong superconvergence of the Euler-Maruyama method for linear stochastic Volterra integral equations, J. Comput. Appl. Math. 317 (2017), 447–457.
[26] H. Tuan, On the asymptotic behavior of solutions to time-fractional elliptic equations driven by a multiplicative white noise, Discrete Contin. Dyn. Syst. Ser. B., 26 (2021), 1749–1762.
[27] T.A. Averina and S.S. Artemiev, Numerical analysis of systems of ordinary and stochastic differential equations, VSP, Utrecht, (1997).
[28] D. Ahmadian and O. Farkhondeh Rouz, Boundedness and convergence analysis of stochastic differential equations with Hurst brownian motion, Bol. Soc. Paran. Mat., 38 (2020), 187–196.
[29] O. Farkhondeh Rouz, D. Ahmadian, and M. Milev, Exponential mean-square stability of two classes of theta Milstein methods for stochastic delay differential equations, AIP Conference Proceedings., 1910 (2017), (060015)-1–(060015)-14.
[30] O. Farkhondeh Rouz, D. Ahmadian, A. Jodaree Akbarfam, and M. Milev, A note on the almost sure exponential stability of the Milstein method for stochastic delay differential equations with Jumps, Int. J. Pure. Appl. Math., 1 (2017), 201–216.
[31] D. Ahmadian and O. Farkhondeh Rouz, Analysis on mean-square and almost sure exponential stability of numerical method for stochastic differential equations with constant delay, Int. J. Appl. Math. Stat., 56 (2017), 1–13.
[32] O. Farkhondeh Rouz and D. Ahmadian, Stability analysis of two classes of improved backward Euler methods for stochastic delay differential equations of neutral type, Comput. Methods Differ. Equ., 5 (2017), 201–213.
[33] D. Ahmadian and O. Farkhondeh Rouz, Mean-square stability of a constructed Third-order stochastic RungeKutta schemes for general stochastic differential equations, Comput. Methods Differ. Equ., 10 (2022), 617–638.
[34] R. Bellman, Stochastic transformations and functional equations, Proc. Sympos. Appl. Math., 16 (1964), 171–177.
[35] E. Hairer, C. Lubich, and M. Schlichte, Fast numerical solution of nonlinear Volterra convolution equations, SIAM. J Sci. Stat. Comput., 6 (1985), 532–541.
[36] R. Gorenflo, A. Kilbas, F. Mainardi, and S. Rogosin, Mittag-Leffler Functions, Related Topics and Applications, Springer-Verlag, Berlin Heidelberg, (2020).
[37] T. Abdeljawad and D. Baleanu, Discrete fractional differences with nonsingular discrete Mittag-Leffler kernels, Adv. Differ. Equ., 2016 (2016), 1–18.
[38] X. Dai and A. Xiao, Levy-driven stochastic Volterra integral equations with doubly singular kernels: Existence, uniqueness and a fast EM method, Adv. Comput. Math., 46 (2020), 1–23.
[39] O. Farkhondeh Rouz, Preserving asymptotic mean-square stability of stochastic theta scheme for systems of stochastic delay differential equations, Comput. Methods Differ. Equ., 8 (2020), 468–479.
[40] T.S. Doan, P.T. Huong, P.E. Kloeden, and A.M. Vu, Euler-Maruyama scheme for Caputo stochastic fractional differential equations, J. Comput. Appl. Math., 380 (2020), Article ID 112989.
[41] M. Li, Ch. Huang, and Y. Hu, Asymptotic separation for stochastic Volterra integral equations with doubly singular kernels, Appl. Math. Letters., 113 (2021), 106880.
[42] W. Zhang, H. Liang, and J. Gao, Theoretical and numerical analysis of the Euler-Maruyama method for generalized stochastic Volterra integro-differential equations, J. Comput. Appl. Math., 365 (2020), 112364.
[43] N. Cong, T. Doan, and H. Tuan, Asymptotic stability of linear fractional systems with constant coefficients and small time-dependent perturbations, Vietnam. J. Math., 46 (2018), 665–680.
[44] A. Wazwaz and R. Rach, Two reliable methods for solving the Volterra integral equation with a weakly singular kernel, J. Comput. Appl. Math., 302 (2016), 71–80.
[45] D. Ahmadian, O. Farkhondeh Rouz, and L.V. Ballestra, Stability analysis of split-step θ-Milstein method for a class of n-dimensional stochastic differential equations, Appl. Math. Comput., 348 (2019), 413–424.

[46] D. Ahmadian and O. Farkhondeh Rouz, Exponential mean-square stability of numerical solutions for stochastic delay integro-differential equations with Poisson jump, J. Inequalities Appl. 186 (2020), 1–33.
[47] Z. Wang, Existence and uniqueness of solutions to stochastic Volterra equations with singular kernels and non-Lipschitz coefficients, Statist. Probab. Lett., 78 (2008), 1062–1071.
[48] X. Zhang, Euler schemes and large deviations for stochastic Volterra equations with singular kernels, J. Differential Equations., 244 (2008), 2226–2250.
[49] X. Dai, W. Bu, and A. Xiao, Well-posedness and EM approximation for nonlinear stochastic fractional integro-differential equations with weakly singular kernels, j. comput. appl. math., 365 (2019), 377–390.
[50] X. Dai, A. Xiao, and W. Bu, Stochastic fractional integro-differential equations with weakly singular kernels: Well-posedness and Euler–Maruyama approximation, Discrete Contin. Dyn. Syst. Ser. B., 27 (2022), 4231–4253.
[51] P.E. Kloeden and E. Platen, Numerical Solution of Stochastic Differential Equations, Springer, (1992).

Faculty of Mathematics, Statistics and Computer Sciences, University of Tabriz, Tabriz, Iran
E-mail: o.farkhonderooz@tabrizu.ac.ir and shahmorad@tabrizu.ac.ir

Department of Mathematics, Van Yuzuncu Yil University, Van, Turkey
E-mail: ferdogan@yyu.edu.tr